Towards Cryophotonics: Experimental Characterization of SOA at Cryogenic Temperatures

Maeva Franco, Pascal Morel, Arnaud Gardelein, and Ammar Sharaiha

***Abstract*—We present an experimental system study of the influence of cryogenic temperatures on the performance of a commercial Semiconductor Optical Amplifier (SOA) over the range 240 K – 70 K. Significant performance improvements were observed when the SOA is in cryogenic conditions. At 70 K and 100 mA we were able to measure a gain as high as 52 dB. At 240 K, only 50 mA of input current are necessary to reach a gain of 37 dB, and a noise figure of 3.8 dB, close to the theoretical limit. The SOA efficiency at power saturation, rises from 2.2% at ambient temperature up to 41% at 100 mA and 120 K.**

***Index Terms*—Amplification efficiency, cryogenic temperatures, gain, noise figure, output saturation power, semiconductor optical amplifier.**

I. Introduction

RECENT research shows that semiconductor optical amplifiers (SOAs) could be an alternative solution for optical amplification in future optical networks [1], [2]. In addition to the amplification of optical signals, SOAs are also used in optical switching and optical signal processing [3], [4], [5]. For all the applications based on SOAs, the system performances depends on the SOA's static and dynamic characteristics such as gain, optical gain bandwidth, output saturation power and noise figure.

Cryogenic environments are often used to reduce noise from detectors [6], for example in infrared imaging applications. The association of photonics and cryogenic temperatures, referred as cryophotonics, can improve the gain (G), noise figure (NF) and amplification efficiency (η) of a SOA.

Several studies on different photonic devices including lasers, SOAs and photodetectors showed that the temperature is a critical parameter which influences the performance [7], [8], [9], [10], [11], [12], [13], [14]. Several investigations focusing mainly on semiconductor lasers have been conducted to extract the temperature dependence of physical parameters such as band gap energy [15], carrier mobility [16], [17], effective masses [18], carrier lifetime [19], internal losses (α) [19] and recombination terms [17], [20], [21]. Under cryogenic conditions, most of the results obtained at material level show performance improvements relative to room temperature. However, to the best of our knowledge, no commercially available SOAs have been evaluated down to cryogenic temperature from a system point of view. It is not obvious to extrapolate a system behavior from the material level study. In this paper, we give the experimental static characterization results for a commercial SOA (CIP SOA-XN-OEC-1550) mounted in a butterfly package for temperatures between 240 K and 70 K. We measured the SOA Amplified Spontaneous Emission (ASE), bias voltage, gain, and output optical power. Other related characteristics such as optical gain, optical gain bandwidth, noise figure, and output saturation power are evaluated based on the measured data. The SOA characteristics at room temperature are given in Table I.

TABLE I
SOA Characteristics Given in the Manufacturer's Datasheet at 293K, 500 mA and 1550 nm

Gain, dB	37.4
PDG, dB	2.3
NF, dB	11.2
P_{sat}, dBm	15.3
Coupling losses, dB	Input facet: 0.8 Output facet: 0.9

II. Presentation of the Cryogenic Testbench and Calibration

A. Cryogenic Setup

Fig. 1 shows a synopsis of the testbench. The SOA is placed inside a cryostat under vaccum (10^{-6} mbar) and connected to a cryocooler (not represented in the synopsis) able to cool the SOA to temperatures from 240 K down to 70 K. The SOA is driven by a DC current source (I_{bias}) in the range 20 mA to 100 mA while a voltmeter monitors its bias voltage (V_{bias}) with

Manuscript received 17 November 2022; revised 16 December 2022; accepted 19 December 2022. Date of publication 26 January 2023; date of current version 31 January 2023. This work was supported in part by Association National de Recherche Technologique ANRT under Grant 2020/0779, and in part by Conseil Départemental Finistère CD29 and Brest Métropole. *(Corresponding author: Maeva Franco.)*

Maeva Franco is with the Air Liquide Advanced Technologies, 38360 Sassenage, France, and also with the Lab-STICC, CNRS, UMR 6285, Ecole Nationale d'Ingénieurs de Brest, 29238 Brest, France (e-mail: maeva.franco@airliquide.com).

Pascal Morel and Ammar Sharaiha are with the Lab-STICC, CNRS, UMR 6285, Ecole Nationale d'Ingénieurs de Brest, 29238 Brest, France (e-mail: morel@enib.fr; sharaiha@enib.fr).

Arnaud Gardelein is with the Air Liquide Advanced Technologies, 38360 Sassenage, France (e-mail: arnaud.gardelein@airliquide.com).

Digital Object Identifier 10.1109/JPHOT.2022.3231651

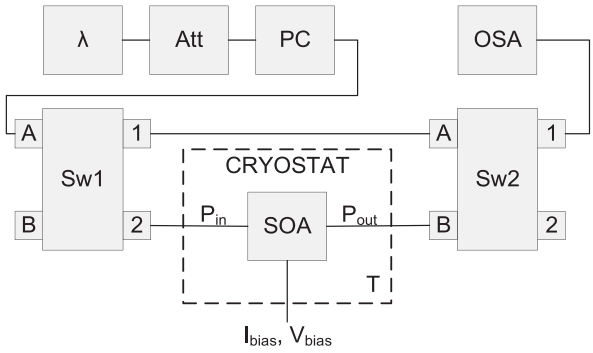

Fig. 1. Synopsis of the cryophotonic test bench. λ represents the tunable laser source, Att is the attenuator, PC the Polarization Controller, Sw1 and Sw2 are 2 × 2 optical switches and the OSA is the Optical Spectrum Analyzer. A cryocooler is connected to the SOA to set the temperature. The SOA is fed by an electrical current I_{bias} while monitoring the bias voltage with a 1 mV precision voltmeter. P_{in} and P_{out} are respectively the measured SOA input and output powers.

1 mV precision. A tunable laser source generates an optical input signal. This is followed by an optical attenuator (Att) used to adjust the SOA input power P_{in}, a polarization controller (PC) and an optical switch (Sw1). The SOA output is connected to the Optical Spectrum Analyzer (OSA) through an optical switch (Sw2). The two switches are used in conjunction to measure the injected optical power at the SOA input (P_{in}) via Sw1 and Sw2 in bar mode while taking into account all the device insertion losses. The ASE power P_{ase} at the SOA ouput is obtained by setting Sw1 in bar mode and Sw2 in cross mode. The ouptut power P_{out} consisting of the amplified input power to which the ASE power P_{ase} is added, is obtained by setting Sw1 and Sw2 in cross mode.

Except for the polarization control, the test bench is fully automated with a python program using in particular numpy [22], matp lotlib [23] and panda [24] libraries. This allows characterization of the ASE, the bias voltage, the gain and the noise figure as functions of the temperature, the bias current, the input power and the wavelength, for minimum and maximum polarizations. The bias current is applied during the cool-down phase. Once the temperature has stabilized (with 0.1 K precision measured in the cryostat) the ASE spectrum is measured without optical signal injection. Since the peak gain shifts with temperature, the study cannot be done at a fixed signal wavelength. We therefore set the signal wavelength for each temperature at the gain peak. We then set the polarization of the optical input signal by minimizing or maximizing the output signal. Finally, we sweep the remaining parameters (wavelength and optical input power). These steps are repeated at several temperatures and then, at several bias currents.

B. Coupling Losses Calibration

As a first approach we computed the gain using the collected raw data. Analyzing the data and specifically the gain spectral shape, we found that the coupling losses inside the SOA butterfly package increased as the temperature decreased due to misalignment of the coupling fiber. We recall here that the SOA we characterized is a commercial SOA, designed to operate between 15°C and 40°C.

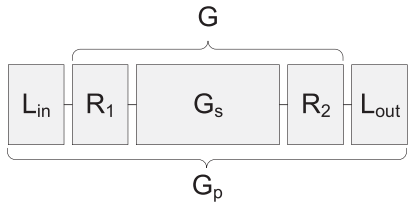

Fig. 2. Model diagram of the SOA packaging. L_{in} and L_{out} are the coupling losses. R_1 and R_2 are the reflection coefficients. G_s is the single-pass gain. G is the gain at chip level. G_p is the gain at package level.

To take into account these temperature-dependent coupling losses, we introduce L_{in} and L_{out} as respectively the input and output coupling losses inside the SOA butterfly package. G is the gain of the SOA chip inside the package considering the single pass gain G_s and the reflectivity coefficients R_1 and R_2. Fig. 2 is a model diagram to illustrate the different terminology mentioned in this paper. The measured output and input power (respectively P_{out} and P_{in}) are then linked by the following equation.

$$P_{out} = P_{in} L_{in} L_{out} G + P_{ase} \tag{1}$$

To estimate the coupling losses at a given temperature, we determine the gain transparency current (I_{tr}) for which the SOA gain is equal to one. I_{tr} is estimated from the measurement of the SOA output power as a function of its bias current for a constant optical input power. I_{tr} is estimated using a first-derivative method based on reference [25]. The cumulative losses in dB ($|10\log(L_{in}L_{out})|$) are extracted from (1) with G = 1.

Fig. 3(a) shows the evolution of the cumulative coupling losses as a function of the temperature. At room temperature the manufacturer's values are 0.8 dB at the input facet and 0.9 dB at the output facet (Table I), whereas we measured a total of 1.5 dB for the two facets. As the temperature decreases the coupling losses increase, as shown in Fig. 3.

The vertical arrows represent the precision of the measures. They have been estimated considering the error we could have made while estimating the bias current. For instance, at 120 K, if we make an error of ± 0.1 mA on the measured bias current, we can make an error of about ± 1.6 dB.

In Fig. 3(b), the measured ASE output spectrums, without signal injection, at both SOA facets show that a slight difference d_{ase} (dB), appears at low temperature unlike at room temperature. This is due to an inhomogeneous coupling fiber misalignment at both SOA facets. d_{ase} is thus related to L_{in} and L_{out} by: $L_{in}(dB) - L_{out}(dB) = d_{ase}$.

C. Polarization Dependent Gain Assessment

The Polarization Dependent Gain (PDG) is enhanced when lowering the temperature. For the studied commercial SOA, the physical reasons of this dependence of polarization on temperature are not well understood as information concerning the structural design is unavailable. In general PDG can be attributed to several parameters such as the confinement factor, mechanical

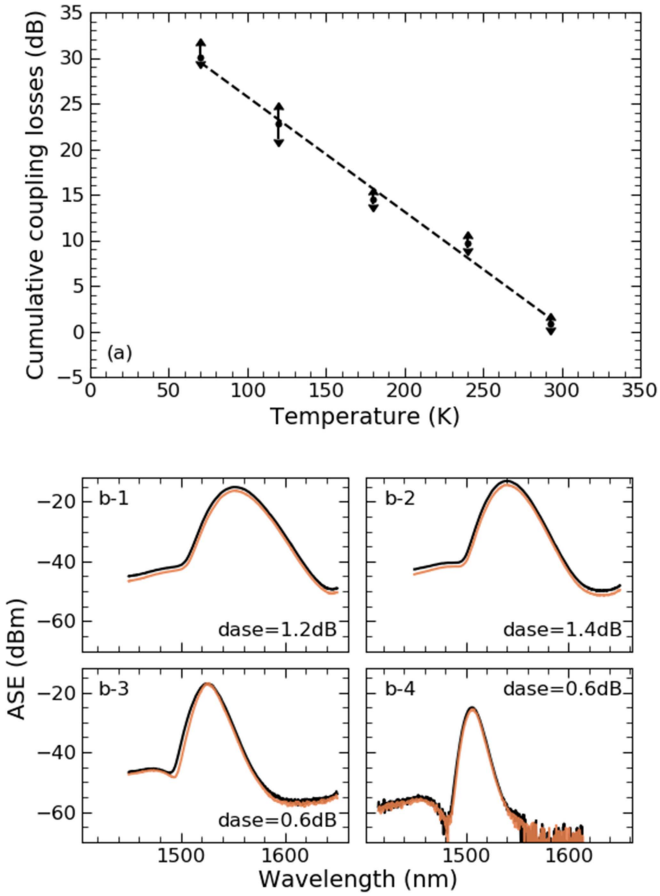

Fig. 3. (a) Cumulative coupling losses (dB). The dots are the values calculated using (1) at $I = I_{tr}$ at each temperature (70 K, 120 K, 180 K, 240 K and 293 K). The dashed line is a linear trendline. (b) ASE spectrum of the SOA at the input (ASEin) in black and output (ASEout) in orange (b-1) at 240 K and 100 mA (b-2) at 200 K and 100 mA (b-3) at 150 K and 50 mA and (b-4) at 70 K and 20 mA. The OSA resolution is set at 0.1 nm.

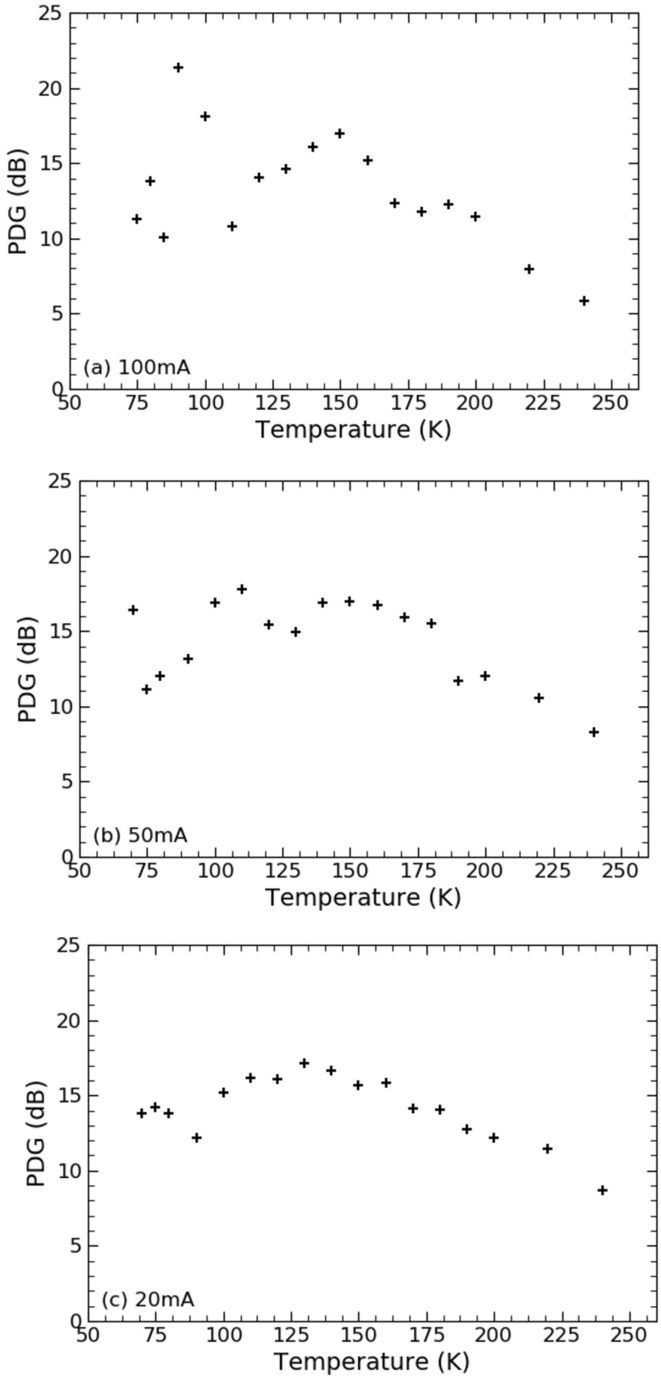

Fig. 4. Polarization dependent gain versus the temperature at (a) 100 mA, (b) 50 mA and (c) 20 mA.

stresses and inhomogeneous thermal strain effects [26], [27]. As we cannot identify TE/TM modes in our fibered setup, we only measured the minimum and maximum gain as a function of the polarization, giving respectively $G_{\min}$ and $G_{\max}$. Fig. 4 presents the evolution of the PDG $G_{\max}(dB) - G_{\min}(dB)$ as a function of the temperature and for three SOA bias currents, for P_{in} = –30 dBm. The PDG reaches a maximum value of about 21.5 dB at 100 mA and 100 K, while for 293 K the datasheet specifies 2.3 dB at 1550 nm, 500 mA, and P_{in} = –30 dBm. This PDG is not negligible and must be taken into consideration when calculating the noise figure. It should be noted that the scatter of the measured PDG points in Fig. 4 is caused by gain ripple (Fig. 7(a), (b)), as described in paragraph III-B-i. In this paragraph, comparing Figs. 4 to 7, the ripple amplitude increases as the scattering of the measured PDG increases.

III. Experimental Results of the SOA Static Characteristics Versus Temperature

In this section we present the results obtained through the static study. Firstly, we discuss the ASE power and the SOA bias voltage. Secondly, after defining the gain G and NF equations, we present their evolution as function of the temperature. Finally, we determine the output saturation power and the power efficiency of the SOA. All these characteristics are given at the SOA chip level.

A. ASE and SOA Voltage

Fig. 5 presents the measured ASE spectrum as a function of the wavelength at different temperatures and without injecting

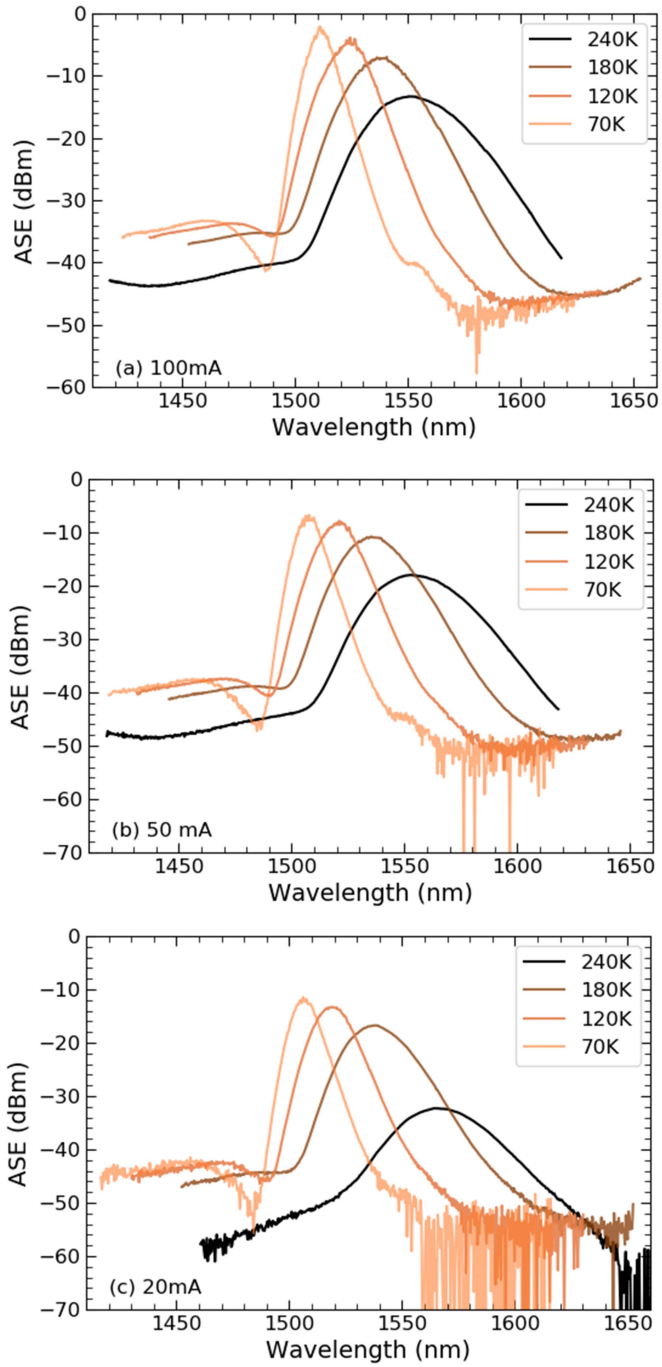

Fig. 5. Amplified spontaneous emission spectrum at various temperatures at (a) 100 mA, (b) 50 mA and (c) 20 mA with an OSA resolution of 0.1 nm.

any optical input power. As the temperature decreases, the ASE peak value increases and shifts towards lower wavelengths and the ASE bandwidth is reduced (from 34 nm at 240 K to 7.5 nm at 70 K at 100 mA). This wavelength shift when lowering the temperature is linked to an increase in the energy bandgap of the semiconductor. This result was expected and was already observed over a smaller temperature range on a semiconductor laser diode [15].

Fig. 6 shows the evolution of the SOA bias voltage V_{bias} as a function of the temperature and bias current. V_{bias} is defined as

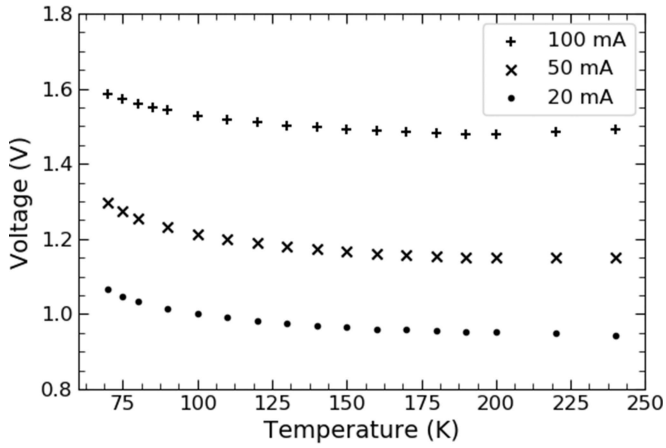

Fig. 6. Bias voltage of the SOA at 100 mA, 50 mA and 20 mA as a function of temperature.

$V_{\text{bias}} = R_i \times I_{\text{bias}} + V_d$, where I_{bias} is the SOA bias current, R_i the resistivity outside the SOA active layer, and V_d the voltage across the SOA active layer. The temperature dependence of V_{bias} arises mainly from the temperature dependence of the carrier mobility which results in R_i being proportional to $T^{3/2}$ [16], [17]. V_d, which is a function of the quasi Fermi levels of the conduction and valence bands, also depends on the temperature [28].

B. Gain, Noise Figure and Output Saturation Power

1) Gain Ripple: When the temperature is lowered, gain ripple appears as visible around the ASE spectrum peak shown in Fig. 5(a). This ripple is related to the residual reflectivities of the SOA cavity where the SOA gain G and the gain ripple depth $\Delta G = \frac{G_{\max}}{G_{\min}}$ are described by (2) and (3) [29], [30]:

$$G = \frac{(1-R_1)(1-R_2)G_s}{\left(1-\sqrt{R_1R_2}G_s\right)^2 + 4\sqrt{R_1R_2}G_s\sin^2(\Phi)} \tag{2}$$

$$\Delta G = \frac{G_{\max}}{G_{\min}} = \left(\frac{1+\sqrt{R_1R_2}G_s}{1-\sqrt{R_1R_2}G_s}\right)^2 \tag{3}$$

where, R_1 and R_2 are the reflectivity coefficients of the SOA cavity, G_s is the single-pass gain, and $\Phi = \frac{2\pi n_e L}{\lambda}$ with L the length of the cavity, n_e the effective index and λ the wavelength.

In Fig. 7(a), we show the measured gain ripple relative to the gain peak wavelength as a function of the temperature. For a SOA bias current of 100 mA, the gain ripple peak to peak amplitude increases as the temperature is reduced and reaches 6.8 dB at 70 K (Fig. 7(b)).

The ripple given by ΔG (3) increases with the gain enhancement for given R_1 and R_2 coefficients.

We also observe an evolution of the periodicity of the ripple with temperature which confirms that a refractive index change occurs in the active layer of the SOA. Assuming a constant length of 3 mm, we can infer a refractive index variation of about -0.05 per Kelvin.

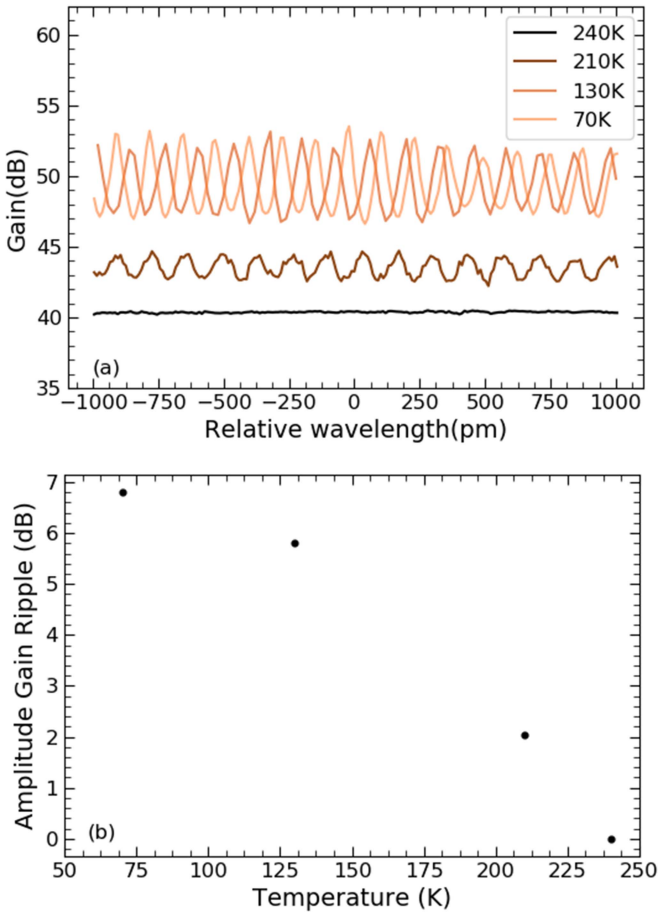

Fig. 7. (a) Gain ripple around the gain peak at 100 mA. From darkest to lightest, the temperatures are 240 K, 210 K, 130 K and 70 K. (b) Amplitude gain ripple as a function of the temperature at 100 mA.

2) Noise Figure Measurement: The noise figure which quantifies the electrical signal to noise ratio degradation of an amplified optical signal in a SOA can be related to its intrinsic parameters and can be expressed in dB at its chip level as follows [31]:

$$NF = 3 + 10\log\left(\frac{\Gamma g}{\Gamma g - \alpha}\right) - 10\log\left(1 - e^{\frac{hc/\lambda - \Delta E_F}{kT}}\right) \quad (4)$$

where Γ the optical confinement in the active layer, g the material gain and α the total internal propagation losses. ΔE_F is the separation between quasi-Fermi levels. hc/λ is the photon energy where λ is the wavelength of the optical input signal. ΔE_F corresponds to the energy where absorption and stimulated emission have the same probability. In the amplification range, we have $hc/\lambda - \Delta E_F < 0$. It has recently been demonstrated that a low and flat NF can be obtained by reducing the term $e^{\frac{hc/\lambda - \Delta E_F}{kT}}$ using high ΔE_F material [31]. Alternatively, the NF can be reduced by reducing the temperature via the two temperature dependent terms in (4). For a constant $hc/\lambda - \Delta E_F$, the exponential term $e^{\frac{hc/\lambda - \Delta E_F}{kT}}$ tends to 0 when the temperature decreases. In addition, α losses in the SOA active region decrease [19] and $10\log(\frac{\Gamma g}{\Gamma g - \alpha})$ tends to 0. Thus, as the temperature is reduced, the calculated NF decreases and could approach the theoretical limit of 3 dB.

TABLE II
GAIN AND NOISE FIGURE AT DIFFERENT CURRENTS AT 293 K. THE DATA AT 500 MA ARE ADAPTED BY CONSIDERING THE COUPLING LOSSES FROM THE DATASHEET. THE DATA AT 85 MA, 50 MA AND 20 MA ARE MEASURED

I (mA)	Gain (dB)	NF(dB)	Wavelength(nm)
500	39.1	10.4	1550
85	15.8	10.1	1570
50	-1.4	15.4	1570
20	High absorption regime		1570

The NF can be experimentally determined at the receiver level using the output ASE power, the gain and the bandpass of the measurement device (in our case, the OSA).

In order to estimate the NF, we use the gain and ASE power at the chip level, including the coupling losses. The gain is obtained from (1):

$$G = \frac{1}{L_{in}L_{out}}\frac{P_{out} - P_{ase}}{P_{in}} \quad (5)$$

where P_{ase} is the ASE mean power measured at the same wavelength as the signal with 0.1nm OSA resolution.

As seen in Section II.C the PDG is not negligible as temperature decreases and has to be considered for the noise factor evaluation. Considering the signal to ASE beating noise and the shot noise, the noise factor for the maximal gain polarization is given by [32]:

$$F_{\max} = \frac{1}{G_{\max}} + \frac{2P_{ase}}{L_{out}G_{\max}\left(1 + \frac{G_{\min}}{G_{\max}}\right)h\nu B_{opt}} \quad (6)$$

where $h\nu$ is the photon energy, B_{opt} the optical resolution of the OSA, $G_{\max}$ and $G_{\min}$ the measured gain for a polarization where the SOA gain is respectively maximized and minimized, and P_{ase}/L_{out} is the chip ASE power in B_{opt} bandwidth under the output signal. L_{out} can be written as $L_{out} = L^{(1/2+\varepsilon)}$ where L are the total losses and ε is the asymmetric ratio between L_{in} and L_{out} with $-1/2 < \varepsilon < 1/2$. Considering $G_{\max} \gg 1$, we can write:

$$F_{\max} \approx \frac{2\,L^{\left(1/2+\varepsilon\right)}P_{ase}}{G_{\max}\left(1 + \frac{G_{\min}}{G_{\max}}\right)h\nu B_{opt}} \quad (7)$$

$$NF = NF_{tot} + \varepsilon \times 10\log(L) = NF_{tot} + d_{ase} \quad (8)$$

with,

$$NF_{tot} = 10\log\left(\frac{2\,L^{1/2}P_{ase}}{G_{\max}\left(1 + \frac{G_{\min}}{G_{\max}}\right)h\nu B_{opt}}\right) \quad (9)$$

Table II gives the gain and the NF at room temperature (293 K) for an input power P_{in} of -30 dBm. The data at 500 mA are

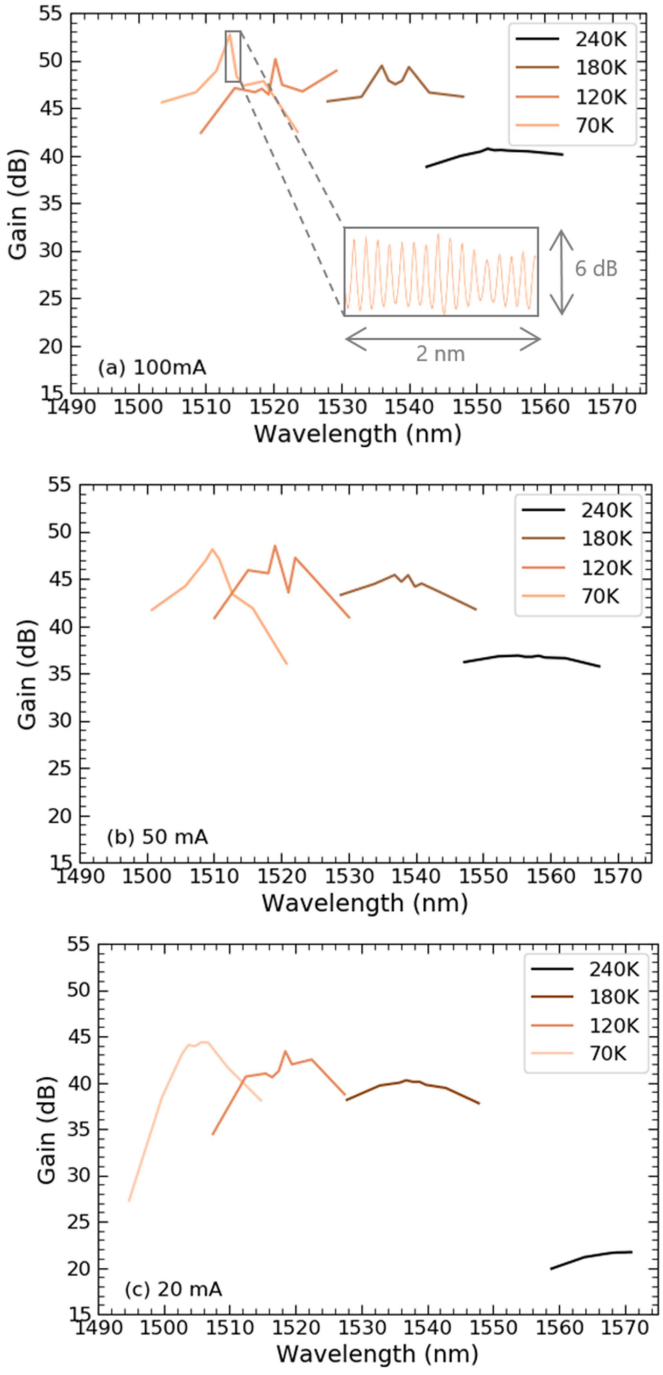

Fig. 8. Gain spectra at (a) 100 mA, (b) 50 mA and (c) 20 mA. From darkest to lightest, the temperatures are 240 K, 210 K, 130 K and 70 K.

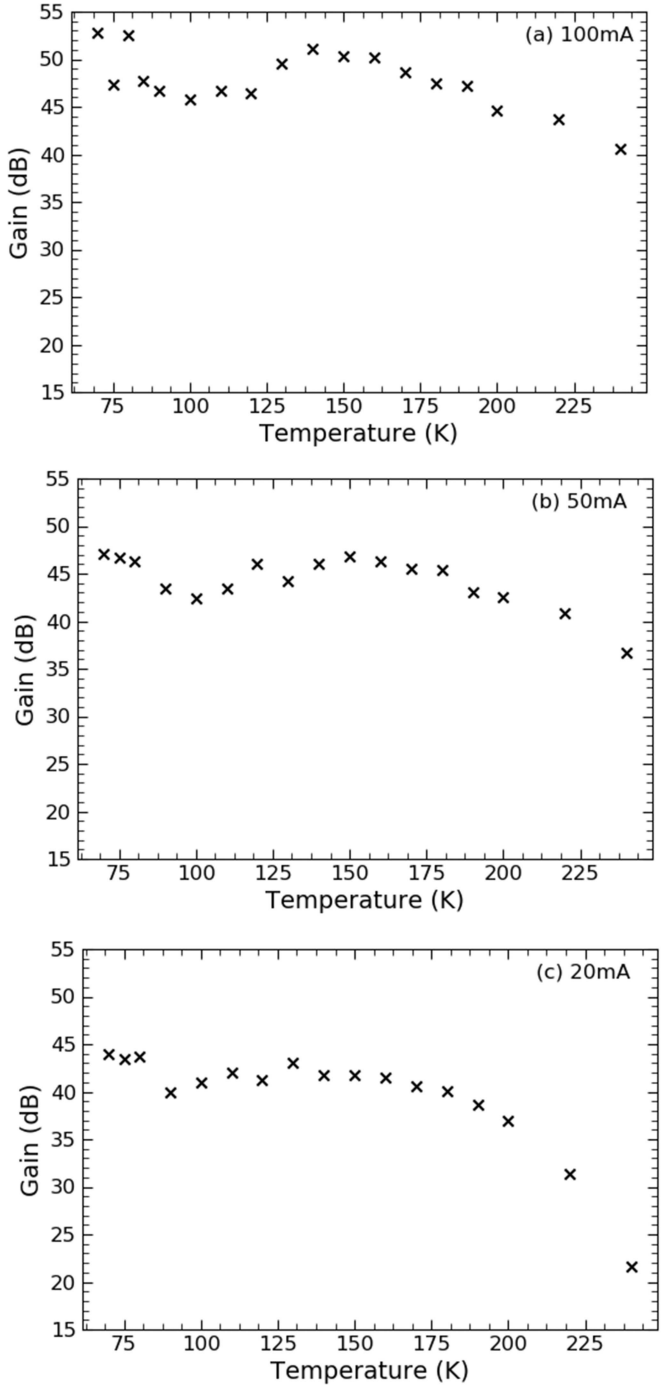

Fig. 9. Gain in dB at (a) 100 mA, (b) 50 mA and (c) 20 mA.

from the datasheet, the ones at 20 mA, 50 mA and 85 mA, are measurements.

3) Gain and Associated Noise Figure: In Fig. 8, we present the gain spectrum at several temperatures (240 K, 180 K, 120 K and 70 K). As observed for the ASE spectrum in Fig. 5, there is a shift towards smaller wavelengths and the bandwidth narrows as the temperature decreases. Moreover, below 180K, gain ripple appears where the gain is much higher. It is due to the residual reflectivities at the SOA facets, which are estimated from (3), of about 10^{-5}. The inset in Fig. 8(a) represents the gain ripple around the gain peak at 70 K.

In Fig. 9, we present the maximal spectral gain value, at several currents (100 mA, 50 mA and 20 mA), for an optical input power $P_{in} = -30$ dBm. The results presented in Fig. 9 are not for a given wavelength. Therefore, the input signal wavelength is adjusted as a function of the temperature and of the current, to follow the gain spectral peak shift. While a constant input power is applied to the butterfly package ($P_{in} = -30$ dBm), the SOA chip input power varies from −32.9 dBm at 240 K to

TABLE III
NOISE FIGURE (DB) ± 0.5 DB IS THE ESTIMATED UNCERTAINTY COMING FROM THE GAIN TRANSPARENCY CURRENT METHOD. THE UNCERTAINTY CAN LEAD TO NF VALUES BELOW THE THEORETICAL LIMIT OF 3 DB WHICH IS IN COMMON USE AS IN [33]

	NF (dB)	
I (mA) \ T (K)	240 K	220 K
100 mA	$\mathbf{4.7 \pm 0.5}$	
50 mA	$\mathbf{3.8 \pm 0.5}$	$\mathbf{4.4 \pm 0.5}$
20 mA	$\mathbf{5.6 \pm 0.5}$	$\mathbf{3.4 \pm 0.5}$

−42.8 dBm at 70 K due to the temperature dependent coupling losses. To obtain the ASE power under the signal as defined in the noise factor definition in (9), we use an averaged ASE power value. This means that above a given gain value, while the output power is impacted by the ripple, the ASE oscillations are smoothed. Therefore we only represented in Table III NF values with SOA gain ripple less than 1 dB corresponding to a maximum gain of about 40 dB.

A first result is that for all three currents the gain increases as the temperature decreases and the calculated noise figure remains below 7 dB. A second result is the reach of a gain as high as 52 dB.

Finally, as discussed in Section III-B-2, the NF decreases as temperature lowers (Table III). We were able to measure the NF only at 240 K and 220 K. As the equation of the NF (9) takes into account the coupling losses, we consider the uncertainty of this measurement on the results of the NF, where the error is indicated in Table III. Such low values very close to the theoretical limit can be attained in conjunction with a high gain. At only 20 mA and at 220 K, a gain of more than 30 dB is obtained with a NF as low as 3.4 dB. As the NF tends towards the theoretical limit at lower temperature, we were not able to estimate accurately the NF value with the current precision measurement method of the coupling losses.

For comparison, at room temperature we can extract from the datasheet (Table I) a gain of 39.1 dB with a noise figure of 10.4 dB for a current of 500 mA. When cooled to 240 K, a bias current of 50mA is enough to reach a gain of 37 dB and a noise figure of 3.8 dB.

Another interesting result is the operating point at 20 mA. At room temperature this current is well below the gain transparency current, thus the SOA is in high absorption regime (Table II). Decreasing the SOA temperature lowers I_{tr} [34] and makes it possible to reach an amplification regime (with a gain of more than 40 dB) with such low currents.

4) Output Saturation Power and Maximum Power: In Fig. 11, we present the gain as a function of the optical output power considering coupling losses, here again at the gain spectral peak. In Table IV, we give both the output saturation power at −3 dB ($P_{-3\text{dB}}$) and the output maximum power ($P_{\max}$). $P_{\max}$ is the maximum output power delivered by the SOA. $P_{-3\text{dB}}$ is the output power corresponding to a 3 dB drop of the gain.

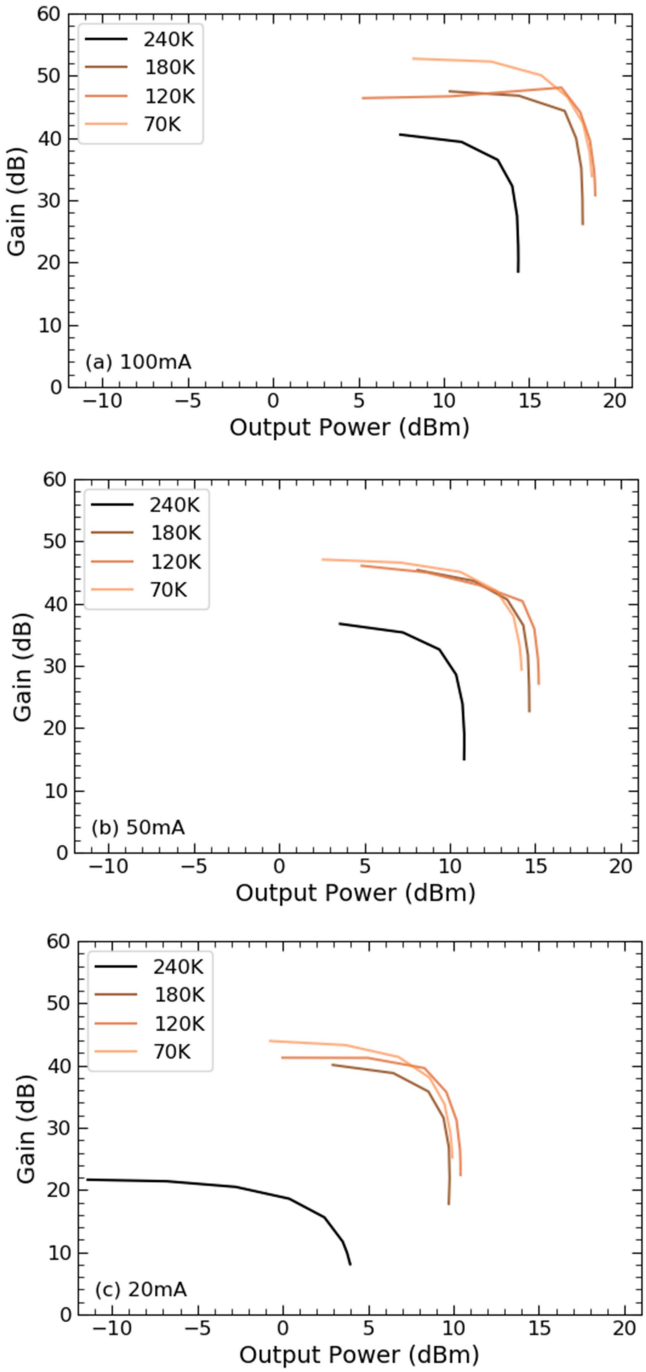

Fig. 10. Gain as a function of the output power at (a) 100 mA, (b) 50 mA and (c) 20 mA. From darkest to lightest colors the temperatures are 240K, 180K, 120K and 70K.

TABLE IV
OUTPUT SATURATION POWER AT −3 DB ($P_{-3\text{ dB}}$) AND OUTPUT MAXIMUM POWER (P_{MAX}) IN DBM FOR 240 K, 180 K, 120 K AND 70 K AT 100 MA, 50 MA AND 20 MA

	P_{-3dB} / P_{max} (dBm)			
I (mA) \ T (K)	240 K	180 K	120 K	70 K
100 mA	**12.4 / 14.4**	**16.8 / 18.1**	**17.7 / 18.9**	**15.9 / 18.7**
50 mA	**8.5 / 10.8**	**12.2 / 14.7**	**11.5 / 15.2**	**11.3 / 14.2**
20 mA	**0.4 / 4.0**	**7.6 / 9.7**	**8.8 / 10.4**	**7.0 / 9.9**

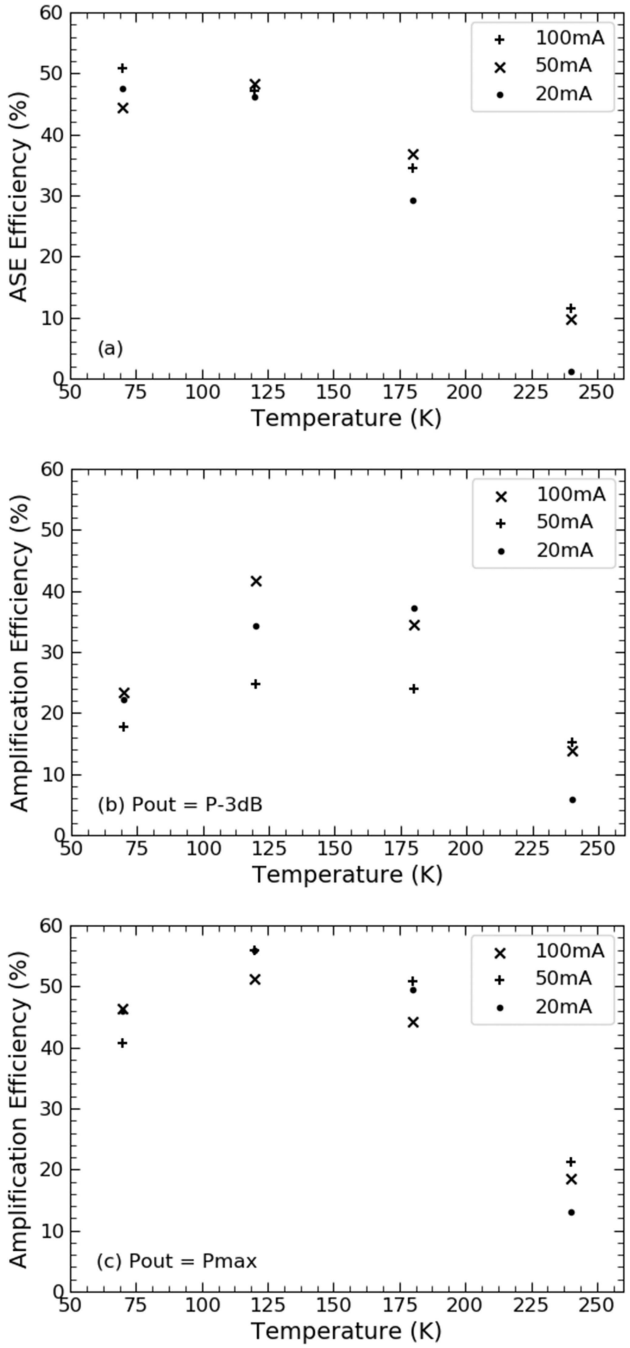

Fig. 11. (a) is the ASE power efficiency as a function of the temperature at 100 mA, 50 mA and 20 mA. (b) and (c) are the power Amplification Efficiency (%) respectively at the output saturation power and the maximum power.

From Table IV, we can see that at a fixed temperature, when the current increases both P_{-3}dB and $P_{\max}$ increase. At a fixed current, down to 120 K, $P_{-3\text{dB}}$ and $P_{\max}$ increase and decrease at 70 K. The constructor's datasheet indicates a saturation power of 15.3 dBm at 293 K and 500 mA which is lower than $P_{-3\text{dB}}$ for temperatures at 180 K, 120 K and 70 K at 100 mA. We measured a saturation power $P_{-3\text{dB}}$ of 16.8 dBm at 180 K and 100 mA. Also, we could reach a maximum output power of 18.9 dBm at 120 K and 100 mA.

C. ASE and Amplification Efficiencies

In the preceding sections, we showed that cryogenic temperatures improve the SOAs static performances in terms of gain, noise figure, and saturation power.

In Fig. 11(a), the ASE power efficiency is defined as $\eta_{ase} = P_{ase}/\ P_{\text{bias}}$ as a function of the temperature, where P_{ase} is the chip total ASE power without injecting optical signal. This shows the increasing electrical-to-optical conversion efficiency when no signal is injected as the temperature is lowered.

We define the power amplification efficiency (η) as being the ratio between the optical output power and the total optical and electrical input power of the SOA. This is similar to what has been done in [35]. However, because P_{in} is small compared to P_{bias}, both definitions are equivalent. The SOA amplification efficiency is given by:

$$\eta = \frac{P_{out} - P_{ase}}{P_{in} + P_{\text{bias}}} \tag{10}$$

where P_{ase} and P_{in} are respectively the chip ASE power and the input optical power. P_{out} is the chip cumulated output optical power including the amplified signal and the ASE at the central wavelength. All the optical powers consider the coupling losses. P_{bias} is the electrical power at the terminals of the SOA with $P_{\text{bias}} = I_{\text{bias}} \times V_{\text{bias}}$.

In Fig. 10 (b) and (c), we show the amplification efficiency as a function of the temperature at 100 mA, respectively at $P_{out} = P_{-3\text{dB}}$ and at $P_{out} = P_{\max}$ using (5). The wavelength is set at the gain spectral peak at each temperature. According to the SOA's datasheet, at 500 mA and 1550 nm, at the saturation power of 15.3 dBm, the efficiency is only 2.19%. However, when cooling the SOA down to 120 K, at 100 mA, the efficiency at $P_{out} = P_{\max}$ increases to about 41%. At maximum power, the efficiency could reach 56% at 120 K and 50 or 20 mA. The remaining power is lost in heat and in the ASE power.

IV. Conclusion

We have been able to show that the SOA temperature is an additional degree of freedom. We showed dramatic improvement of the system performances in cryogenic conditions, allowing new applications for this component. The main results were a) a gain as high as 52 dB at 70 K and 100 mA; b) a very low noise figure of 3.4 at 220 K and 20 mA close to the theoretical limit of 3 dB; c) a higher saturation power $P_{-3\text{dB}}$ of 17.7 dBm at 120 K with only 100 mA versus 15.3 at room temperature and 500 mA; d) a high maximum power of 18.7 dBm at 100 mA and 70 K; e) a SOA efficiency of 41% at 120 K, 100 mA and $P_{out} = P_{-3\text{dB}}$ versus 2.2% at room temperature and 500 mA. In addition to the mentioned improvements, the spectral amplification window is modified. We observe a blue shift of the peak gain wavelength as well as the narrowing of the spectra when the temperature is lowered. These results demonstrate the potential for the association of photonics and cryogenics in a discipline we refer to as cryophotonics.

Such results were obtained with a commercial SOA designed to operate at room temperature, resulting in increasing coupling losses, gain ripple and PDG as the temperatures lowers. We could benefit from the conception of a SOA designed for cryogenic environment use. In particular, the coupling losses should be optimized for the required cold temperature by developing appropriate alignment procedures or material selection [36], [37]. For the gain ripple, since the device delivers high gains at cold temperatures, the residual reflection coefficient should dramatically be reduced below our estimation of 10^{-5}, in order to be adapted to higher gains. Finally the PDG could be minimized by optimizing the design of strained SOAs at the desired temperature.

Cryophotonics pave the way for new applications of SOA such as Low Noise SOAs or very high switching extinction ratio with low bias current variation.

ACKNOWLEDGMENT

We would like to thank James Butterworth for his advices and fruitful conversations.

REFERENCES

[1] R. Bonk, "SOA for future pons," in *Proc. IEEE Opt. Fiber Commun. Conf.*, 2018, pp. 1–3.
[2] J. Zhang et al., "56 Gbit/s/λ PAM-4 IM/DD transmission over 120 km SSMF at O-band using cascaded semiconductor optical amplifiers for data center interconnects," in *Proc. IEEE Asia Commun. Photon. Conf.*, 2020, pp. 1–3.
[3] A. Boucouvalas, K. Peppas, K. Yiannopoulo, and Z. Ghassemlooy, "Underwater optical wireless communications with optical amplification and spatial diversity," *IEEE Photon. Technol. Lett.*, vol. 28, no. 22, pp. 2613–2616, Nov. 2016.
[4] X. Zhang, T. Cao, and W. Dong, "Engineering nonlinear effects of quantum-well semiconductor optical amplifiers for applications in optical signal processing," *IEEE J. Sel. Topics Quantum Electron.,* vol. 29, no. 6, Nov./Dec. 2023, Art. no. 7600311.
[5] D. Kastritsis, T. Rampone, M. Franco, K. Zoiros, and A. Sharaiha, "SOA-MZI photonic sampler with a post-distortion linearization technique," *Opt. Exp.*, vol. 29, no. 15, pp. 23736–23751, 2021.
[6] B. Wiecek, "Cooling and shielding systems for infrared detectors - requirements and limits," in *Proc. IEEE Eng. Med. Biol. 27th Annu. Conf.*, 2005, pp. 619–622.
[7] O. Eyal et al., "Static and dynamic characteristics of an InAs/InP quantum-dot optical amplifier operating at high temperatures," *Opt. Exp.*, vol. 25, no. 22, pp. 27262–27269, 2017.
[8] G. Liu et al., "Temperature-dependent gain characteristics of InAs/InP quantum dash semiconductor optical amplifiers," in *Proc. IEEE Photon. North*, 2020, pp. 1–1.
[9] K. Lau, C. Harder, and A. Yariv, "Direct modulation of semiconductor lasers at f10 GHz by low-temperature operation," *Appl. Phys. Lett.*, vol. 44, no. 3, pp. 273–275, 1984.
[10] P. Crump et al., "85% power conversion efficiency 975-nm broad area diode lasers at -50°C, 76% at 10°C," *Opt. Soc. Amer.*, pp. 1–2, 2006, doi: 10.1109/CLEO.2006.4628740.
[11] D. Bown, "The promise of cryogenic solid-state lasers," *IEEE J. Sel. Topics Quantum Electron.*, vol. 11, no. 3, pp. 587–599, May/Jun. 2005.
[12] Y. Zhang, V. Borzenets, N. Dubash, T. Reynolds, Y. Wey, and J. Bowers, "Cryogenic performance of a high-speed GaInAs/InP p-i-n photodiode," *J. Lightw. Technol.*, vol. 15, no. 3, pp. 529–533, Mar. 1997.
[13] Y. Kumar and M. Shenoy, "Enhancement in the gain recovery of a semiconductor optical amplifier by device temperature control," *Pramana – J. Phys.*, vol. 87, no. 6, pp. 1–6, 2016.
[14] P. Borri et al., "Exciton relaxation and dephasing in quantum-dot amplifiers from room to cryogenic temperature," *IEEE J. Sel. Topics Quantum Electron.*, vol. 8, no. 5, pp. 984–991, Sep./Oct. 2002.
[15] S. Vlasova, A. Vlasov, K. Alloyaroy, and T. Volkova, "Investigation of the temperature dependence of the radiation from semiconductor lasers and light emitting diodes," in *Proc. 5th IOP Conf. Earth Environnement Sci.*, vol. 539, 2020, Art. no. 012137.
[16] B. Streetman and S. Banerjee, *Solid State Electronic Devices*, 7th ed. London, U.K.: Pearson, 2016, pp. 120–127.
[17] E. Rosencher and B. Vinter, *Optoélctronique*, 2nd ed. Dunod, 2002.
[18] V. Gopal, "Temperature dependence of effective mass of electrons & holes and intrinsic concentration in silicon," *Indian J. Pure Appl. Phys.*, vol. 20, pp. 180–182, 1982.
[19] M. Asada and Y. Suematsu, "The effects of loss and nonradiative recombination on the temperature dependence of threshold current in 1.5-1.6 μm GaInAsP/InP lasers," *IEEE J. Quantum Electron.*, vol. 19, no. 6, pp. 917–923, Jun. 1983.
[20] T. Trupke et al., "Temperature dependence of the radiative recombination coefficient of intrinsic crystalline silicon," *J. Appl. Phys.,* vol. 94, no. 8, pp. 4930–4937, 2003.
[21] R. Brüggemann, M. Xu, J. Alvarez, M. Boutchich, and J. Kleider, "Temperature dependence of the radiative recombination coefficient in crystalline silicon by spectral and modulated photoliuminescnences," *Physica Status Solidi*, vol. 11, no. 6, 2017, Art. no. 1700066.
[22] C. Harris et al., "Array programming with NumPy," *Nature*, vol. 585, no. 7825, pp. 357–362, 2020.
[23] J. Hunter, "Matplotlib: A 2D graphics environment," *Comput. Sci. Eng.,* vol. 9, no. 3, pp. 90–95, May/Jun. 2007.
[24] W. McKinney, "Data structures for statistical computing in Python," in *Proc. 9th Python Sci. Conf.*, 2010*,* pp. 51–56.
[25] T. Hertsens, "Application note: An overview of laser diode characteristics. Measuring diode laser characteristics," *ILX Lightw.*, pp. 1–7, 2005.
[26] S. Pajarola, J. Eckner, P. Besse, G. Guekos, and D. Syvridis, "Temperature behavior of a bulk InGaAsP/InP ridge waveguide structure for polarization insensitive optical amplifier operation," *Appl. Phys. Lett.*, vol. 65, no. 22, pp. 2762–2764, 1994.
[27] P. Jayavel et al., "Optical polarisation properties of InAs/GaAs quantum dot semiconductor optical amplifier," *Jpn. Soc. Appl. Phys.,* vol. 44, no. 4S, pp. 2528–2530, 2005.
[28] B. Sapoval and C. Hermann, "Physique des semi-conducteurs," in *Ellipses*, 1990.
[29] Y. Yamamoto, "Coherence, amplification, and quantum effects in semiconductor lasers," *Wiley Intersciences*, vol. 7, pp. 272–273, 1991.
[30] M. J. Connelly, "Wideband semiconductor optical amplifier steady-state numerical model," *IEEE J. Quantum Electron.*, vol. 37, no. 3, pp. 439–447, Mar. 2001.
[31] S. Yu et al., "Flat noise figure semiconductor optical amplifier," in *Proc. IEEE Eur. Conf. Opt. Commun.*, 2021, pp. 1–3.
[32] T. Briant, P. Grangier, R. Tualle-Brouri, A. Bellemain, R. Brenot, and B. Thédrez, "Accurate determination of the noise figure of polarization-dependent optical amplifiers: Theory and experiment," *J. Lightw. Technol.,* vol. 24, no. 3, pp. 1499–1503, Mar. 2006.
[33] L. Belostotski and J. W. Has, "Evaluation of tuner-based noise-parameter extraction methods for very low noise amplifiers," *IEEE Trans. Microw. Theory Techn.,* vol. 58, no. 1, pp. 236–250, Jan. 2010.
[34] J. Pankove, "Temperature dependence of emission efficiency and lasing threshold in laser diodes," *IEEE J. Quantum Electron.,* vol. 4, no. 4, pp. 119–122, Apr. 1968.
[35] J. Plant, A. Goyal, D. Oakley, D. Chapman, A. Napoleone, and P. Juodawlkis, "Improving the efficiency of high-power semiconductor optical amplifiers," in *Proc. Opt. Soc. Amer. Proc. Conf. Lasers Electro-Opt.*, 2008, pp. 1–2.
[36] T. Lay, H. Yang, C. Lee, and W. Cheng, "Fiber grating laser: A performance study on coupling efficiency of fiber microlens and the Bragg reflictivity," *Opt. Commun.*, vol. 233, pp. 89–96, 2004.
[37] D. Lee, R. Haynes, and D. Skeen, "Properties of optical fibres at cryogenic temperatures," *Monthly Notices Roy. Astronomical Soc.*, vol. 326, pp. 774–780, 2001.